Materials Research Bulletin 154 (2022) 111930

Contents lists available at ScienceDirect

Materials Research Bulletin

journal homepage: www.elsevier.com/locate/matresbu

Research Papers

High transparent wood composite for effective X-ray shielding applications

Nurul Awaliyah Muhammad, Bidayatul Armynah, Dahlang Tahir *

Department of Physics, Hasanuddin University, Makassar 90245, Indonesia

ARTICLE INFO

Keywords:
Transparent wood
X-ray shielding
PVA
Gelatin
Radiation
Barium carbonate

ABSTRACT

The flexible and transparent film for X-ray radiation shielding have been fabricated successfully in the form of composites PVA/Gelatin/$BaCO_3$/transparent wood. The wood samples were delignified for 3, 6, and 9 h to remove the lignin content. Beer-Lambert equation was used to calculate the shielding parameter based on the thickness of the sample and the intensity before and after applied all energy irradiation considered. FTIR and X-ray shielding test confirmed that the shielding able to absorb most of photon energy and well-interacting with atoms in samples. Low HVL shows the material was effectively block the radiation. The samples with 0.5 g $BaCO_3$ showed the lowest HVL (0.72747 cm) compared to others composition. The linear attenuation coefficient was 1.37463 cm^{-1} at 55 keV with of 0.5 g of $BaCO_3$. The mass attenuation coefficient also confirmed that the attenuation of composites increases (ex. 55 keV irradiation energy for 0.1 g $BaCO_3$ is 0.793, 0.941 cm^{-1} for 0.3 g $BaCO_3$, and 1.115 cm^{-1} for 0.5 g $BaCO_3$) linearly along with increasing of $BaCO_3$ concentration and shows good agreement with theoretical calculation from XCOM database. It is indicated that the PVA/Gelatin/$BaCO_3$/transparent wood composites show high potentials as a new transparent and flexible shielding material for X-ray radiation application in medical sector.

1. Introduction

The application of electromagnetic wave radiation including X-rays, gamma rays and nuclear radiation has been widely used in the health sector, such as diagnosis, surgery and radiotherapy [1–3]. The energy range of X-rays was 10 eV to 100 keV [4]. Radiation workers or patients are at risk of receiving excessive radiation, which can cause health problems such as body tissue damage, fatigue, nausea, vomiting, hair loss, headache, diarrhea, cell mutations, cancer and even death [5,6]. Therefore, radiation shielding materials are required to minimize the intensity of radiation exposure by applying materials to absorb or scatter radiation from a radiation source. The radiation shield must absorb at least 50% of the given radiation intensity [7,8]. The radiation also requires to have a high photon attenuation coefficient to obtain the best intensity reduction [9].

Generally, radiation shields that have been used are lead (Pb) [10,11] since X-ray radiations required high atomic number but for Pb toxic to living things and the environment. Nowadays mainly protected the X-ray radiography operators in medical or industrial by transparent structure Pb compound. However, Pb also is dangerous for health and forbid the use of Pb compound in near future by the International Commission Radiation Protection (ICRP) [12,13]. Several types of metals such as bismuth (Bi) [14–18], tungsten (W) [19,20], and barium (Ba) [7,21,22] are materials that are often used to replace Pb. Some reported research composite containing bismuth have been employed for shielding purposes due to high atomic number: bismuth trioxide and EPDM rubber as reported by Gungor et al. [15] composite polydimethylsiloxane/Bismuth (III) oxide as reported by Yilmas et al. [16], both synthesized by vulcanization method, and composite PVC/Bi_2O_3 was synthesized by simple mechanical stirring [17]. Tishkevich et al. [18] reported that the unique properties of Bi coated with gelatin synthesized by electrochemical method and shows increasing dose X-ray absorbed by the shield. Other composite also reported by Tishkevich et al. [20] using tungsten for alternative shielding which was synthesized by solid phase method.

The composite combination between barium and bismuth also was reported in the form of barium-doped PVC/Bi2WO6 synthesized by simple mixing and then continue stirring as reported by Gholamzadeh et al. [23]. Barium sulfate ($BaSO_4$) as an X-ray radiation shielding material purposes was reported by Jiang et al. [7] and Thongpool et al. [21] and showed an increase of attenuation coefficient along with increase of barium concentration. Jaiyen et al. [22] also showed similar results, where the best radiation shielding ability was achieved when the barium concentration was higher. This can be caused by the interaction of

* Corresponding author.
E-mail address: dtahir@fmipa.unhas.ac.id (D. Tahir).

https://doi.org/10.1016/j.materresbull.2022.111930
Received 12 October 2021; Received in revised form 15 May 2022; Accepted 9 June 2022
Available online 11 June 2022

X-rays with the atoms of the absorbent material which is relatively higher because of the denser particles [19]. Another study by Kalkornsurapranee et al. [6] showed a comparison of the effectiveness of barium carbonate ($BaCO_3$) and barium sulfate ($BaSO_4$) as a radiation shield, where $BaCO_3$ is high ability to attenuate photon due to the higher mass attenuation coefficient and lower half value layer (HVL) which than that of $BaSO_4$. These results also show a conformity with the linear attenuation coefficient of $BaCO_3$ which is lower than of $BaSO_4$, moreover, $BaCO_3$ has excellent electronic properties due to its oxide materials. This was reported by Trukhanov et al. [24], barium hexaferrite synthesized by solid state method shows good magnetic and electronic properties or magneto-electronic at room temperature. Furthermore, other ferrites which is complex iron oxides materials with similar characteristics deposited by electrochemical method was studied by Zdorovets et al. [25]. Then, other new methods for synthesis functional oxide nanomaterials have been developed was by Almessiere et al. [26] using citrate gel process, simple green synthesis reported by Thakur et al. [27], and electrolyte deposition methods for thin films reported in 2019 by Zubar et al., [28,29].

However, the existing radiation shielding material has several disadvantages such as less plasticity and flexibility because it comes from a rigid solid. Metal-polymer composites can be a good deal as flexible radiation shielding [7,8,30]. Jiang et al. [7] obtained that metal-polymer composites of barium sulfate (BaSO4)/cellulose can be used as radiation shields. In addition, Yakubu et al. [31] shows a study of wood-polymer composites that can also be used as radiation shields. Furthermore, Aggrey-Smith et al. [9] also found that several types of tropical wood can be used as radiation shielding materials in the energy range of 50–150 keV and if metal materials are added, as in the study of Poltabtim et al. [32], the linear attenuation coefficient and mass attenuation coefficient increased within increasing metal concentration but decreased as photon energy increased. The same result also obtained by Ozkan [33] when pine wood was added with boric acid.

In line with previous research by Aggrey-Smith et al. [9,31–33], normal wood is very effective to absorbing and scattering light [34] but it is not transparent. Since the X-ray operators need also to see what they are doing, the X-ray shield also should be transparent to the visible light. To obtain transparent wood, chemical treatment was the easy way to minimize or eliminate the lignin content as the dominant element caused wood impurity. This treatment called delignification [35,36]. Ref. [36] showed that of hydrogen peroxide (H_2O_2) increased optical transmission more than 44% as the delignification time increased. Some delignification solutions that are often used by researchers are NaOH [37], Na_2SO_3 [38] H_2O_2 [36], $NaClO_2$ and CH_3COOH [39,40]. However, transparent wood has fewer mechanical properties as the lignin content decreases, so it needs to be reinforced with polymers to obtain good flexibility.

Polymers such as polyvinyl alcohol (PVA) have often been used as polymer matrices because they are more environmentally friendly, easily soluble in water and good transparency [41,42]. Besides PVA, gelatin is also a natural polymer that is easy to obtain and environmentally friendly [43] where well known that, the combination of different compounds that have excellent electronic properties leads to new composite materials which have earned great technological interest in recent years in the pharmaceutical and industrial fields [44,45]. The addition of gelatin to PVA will produce new composite material as a second phase as reported recently by Korolkov et al. [46]. By the additional of polymer also will improving electrochemical detection of metal ion and affected significantly to the electronic properties. In fact, gelatin was very easy to mold, so it required to add other binding agents such as PVA to keep it durable [47]. In addition, PVA has been used as a matrix of metallic materials to fabricate new materials for radiation shielding [14,19,21,48,49]. In a study of Ebnalwaled and Ismaiel [50], showed that PVA/Gelatin was well-interact as a radiation shielding.

Transparent wood has been developed as new biocomposite material with good transmission and mechanical properties. The type of wood have been reported was basswood [36,40,51], poplar wood [37,52], balsa wood [38,53–55], pine wood [56], birch wood [39,57], beech wood [58,59], Betula alnoides, Chinese fir, New Zealand pine, oguman, and black walnut [60]. As long as our knowledge, there is no reported for Sonokeling or Indian rosewood for new application as a flexible and transparent shielding of the X-ray radiation which has uniform texture and easy to grow in Indonesia indicated that high availability. By combining different types of polymers with oxides and carbon-based materials, as reported Yakovenko et al. [61] and Yakovenko et al. [62] using barium hexaferrite-epoxy composite polymerization with carbon nanotube, the new composites with increase and attractive electronic properties could be fabricated.

Hence, in this study, the delignification process on Sonokeling wood veneers using H_2O_2 solution with heating time of 3, 6, and 9 h, respectively, and fabricate transparent wood composites using PVA/Gelatin polymer doped with Barium Carbonate ($BaCO_3$) as a new composite of X-ray radiation shielding. Then, the shielding ability will be compared to theoretical database XCOM from National Institute of Science and Technology (NIST). The chemical composition also will be characterized by Fourier Transform Infrared (FTIR) and testing the shielding ability using X-ray mobile.

2. Experimental section

2.1. Chemicals and materials

The chemicals: H_2O_2 50%, ethanol, HCl 0.1 M, $BaCO_3$, and PVA, all was purchased from Merck Chemical Co. (99.9% purity) KGaA, Darmstadt, Germany. Gelatin was obtained from local company by Msmart-Shop bloom 140 mesh 20, Indonesia. The Sonokeling or Indian rosewood veneers was measured in 10×10 cm dimension supplied from local company by Kreasi Veneer Indonesia.

2.2. Wood delignification

Wood delignification process was follows [36]. Wood veneers were immersed in delignification solution of hydrogen peroxide and heated in microwave at 60 °C with adjusting treatment time of 3, 6, and 9 h. After delignification, the wood samples were submerged in ethanol to remove the chemical residual and stored for further treatment (Fig. 1).

2.3. Fabrication transparent shielding film

PVA (10 w/v %) and gelatin (20 w/v %) solution were prepared using sol-gel method [37], as shown in Fig. 2. An aqueous solution of PVA/Gelatin were mixed and stirred for 60 min. Then, three levels of barium carbonate were added to PVA/Gelatin solution; 0.1, 0.3, and 0.5 g (in which prepared by dissolving in HCl (0.1 M) for every level). The mixture was stirred for 60 min and formed shielding solution then molded. The wood veneer was sandwiched between the shielding solutions and heated 20 h. Let it dry in room temperature for 2 days then peeled off. After that, the dried transparent wood shielding composites ready for characterization. The Thickness and density of composite PVA/Gelatin/Transparent Wood/$BaCO_3$ for different delignification time as shown in Table 1.

The synthesized methods were dependent on the materials, for composite containing polymer such PVC was reported by mechanical stirring method [17] and for polymer such EPDM rubber and polydimethylsiloxane was synthesized by vulcanization method [15,16]. For functional oxide materials were synthesized by various new methods such as: $[Ni_{0.5}Co_{0.5}](Dy_xFe_{2-x})O_4$ ($x \leq 0.08$) by citrate gel process [26], barium ferrite (BaFe12O19) nanoparticle by green technology [27], and NiFe nanocrystalline films on Au film by pulsed electrolyte deposition [28,29] (Tables 2 and 3).

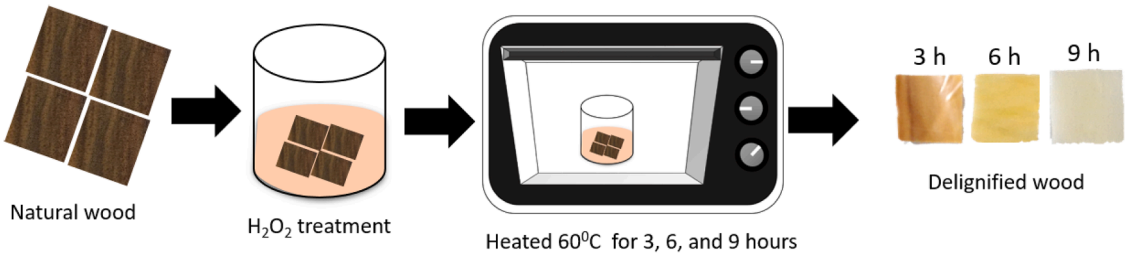

Fig. 1. Schematic illustration of delignification process in this study.

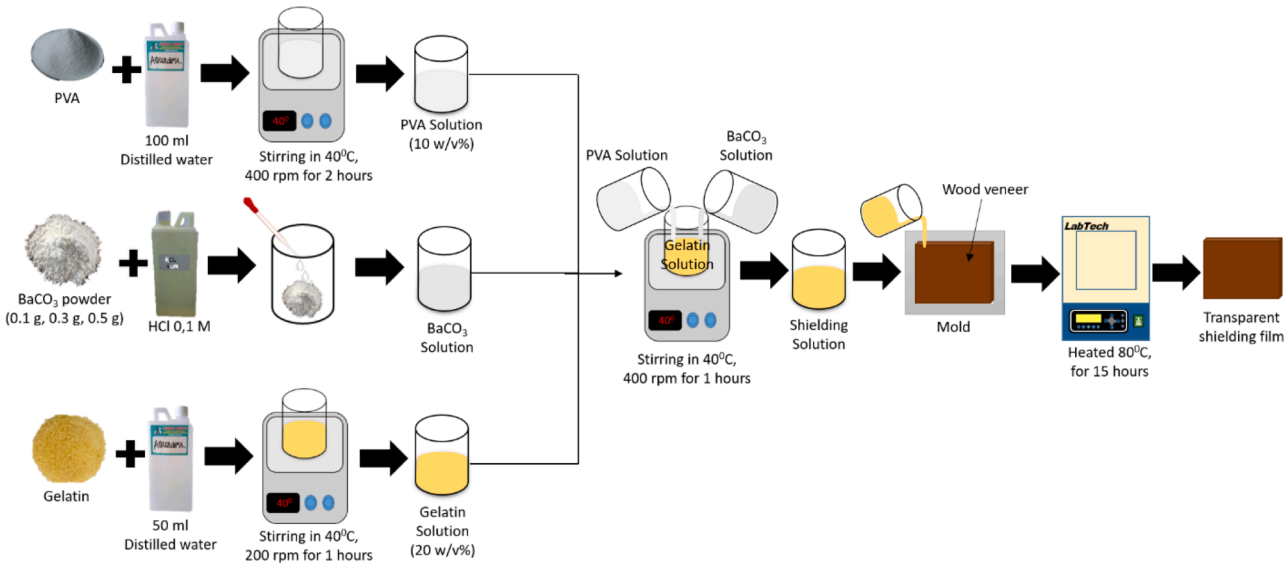

Fig. 2. Illustration of transparent shielding film fabrication of composite PVA/Gelatin/$BaCO_3$/wood in this study.

Table 1
The thickness of composite PVA/Gelatin/transparent wood without and with additional $BaCO_3$ for different delignification time (3, 6, and 9 h).

Samples	Delignification time (h)				Density (g. cm^{-3})
	0	3	6	9	
	Thickness (cm)				
Normal Wood	0.104	-	-	-	0.010
PVA/Gelatin/Transparent Wood	2.27	-	-	-	0.189
PVA/Gelatin/Transparent Wood/0.1 $BaCO_3$	2.28	2.16	1.74	1.62	0.195
PVA/Gelatin/Transparent Wood/0.3 $BaCO_3$	2.31	2.22	1.63	1.43	0.214
PVA/Gelatin/Transparent Wood/0.5 $BaCO_3$	2.35	2.17	1.45	1.23	0.223

2.4. Characterization

The wood veneers chemical composition was characterized using Fourier transform infrared (FT-IR) from Shimadzu Corp Japan, type IRPrestige-21 in the wavenumber range 3700–600 cm^{-1}.

2.5. X-ray shielding test

The X-ray shielding test was measured in Health Facility Safety Center (BPFK), Makassar, Indonesia, using a mobile X-Rays for 9 times irradiation with energy 55, 66, 77, and 90 keV, 10 mAs. These types of energies used to release photon for radiation to get image from thorax, abdomen, head, and neck based on the ICRP [12,13]. The sample was placed under the X-ray tube with the distance between the source and sample is 1 m and the collimator set by area of 4 x 4 cm then irradiated. After irradiated, the detector will show the initial and irradiated intensity data. The data will be counted using Beer-Lambert equation to calculate the shielding parameters.

3. Results and discussion

3.1. Transparent shielding film composite

During the delignification process, the wood veneers were treated with hydrogen peroxide for 3, 6, and 9 h to remove the lignin content. As shown in Fig. 3, the removal lignin content showed by changing in color of the wood veneer from dark brownish (natural wood) to yellowish (3 h), and then brighter (6 h) to white (9 h). Theoretically, the longer delignification time means the more lignin is loses, the more porosity in wood cells, the more space to fill by polymer, before it saturated [56]. The delignification makes wood become weaker due to the loss of lignin, its mean the mechanical properties decreased [40]. Normal wood is very effective to absorbing and scattering light due to the presence of lignin. The delignified wood was not transparent either, but delignification increase the light attenuation [34,54].

Subba Rao et al. [37] shows that delignification process will form pores or crack in wood cells that related to low mechanical properties. To increase the mechanical properties, the polymer (PVA/Gelatin) was added to the wood veneers [63]. The polymers will fill the pores and interacted with the cellulose nanofibrils in wood cells. This interaction resulting in increased flexibility and transparency of the composite, and it will be able to bend without breaking the fiber. Polymers not only fill the pores, but also penetrate in wood cells so that the wood cells will be more tightly bonded resulting composite with good flexibility [36].

Table 2
The linear attenuation coefficient (cm^{-1}) from experimental results (EXP) of composite PVA/Gelatin/Transparent Wood with additional $BaCO_3$ (0.1, 0.3, and 0.5 g) for various delignification time (3, 6, and 9 h) and energy of the X-ray sources (55, 66, 77, and 90 keV). We have included theoretical calculation from XCOM database for comparison.

$BaCO_3$ additives	Delignification time	Mass attenuation coefficient (cm^2g^{-1})							
		55 keV		66 keV		77 keV		90 keV	
		EXP	XCOM	EXP	XCOM	EXP	XCOM	EXP	XCOM
0 g	0 h	0,348	0,323	0,240	0,257	0,182	0,2	0,161	0,174
0.1 g	3 h	4,219	5,039	2,936	3,135	2,077	2,109	0,995	1,421
	6 h	3,781		2,952		1,913		1,467	
	9 h	4,066		3,052		1,981		1,504	
0.3 g	3 h	4,828		3,014		2,265		1,663	
	6 h	2,952		1,913		1,467		4,076	
	9 h	3,052		1,981		1,504		4,397	
0.5 g	3 h	6,164		3,402		2,918		1,928	
	6 h	1,913		1,467		4,076		3,115	
	9 h	1,981		1,504		4,397		3,998	

Table 3
The mass attenuation coefficient (cm^2g^{-1}) from experimental results (EXP) of composite PVA/Gelatin/Transparent Wood with additional $BaCO_3$ (0.1, 0.3, and 0.5 g) for various delignification time (3, 6, and 9 h) and energy of the X-ray sources (55, 66, 77, and 90 keV). We have included theoretical calculation from XCOM database for comparison.

$BaCO_3$ additives	Delignification time	Linear attenuation coefficient (μ) (cm^{-1})							
		55 keV		66 keV		77 keV		90 keV	
		EXP	XCOM	EXP	XCOM	EXP	XCOM	EXP	XCOM
0 g	0 h	0,048	0,04	0,033	0,032	0,025	0,029	0,022	0,025
0.1 g	3 h	0,823	1,079	0,573	0,642	0,405	0,457	0,194	0,274
	6 h	0,737		0,576		0,373		0,286	
	9 h	0,793		0,595		0,386		0,293	
0.3 g	3 h	1,033	0,983	0,645	0,585	0,485	0,416	0,356	0,249
	6 h	0,872		0,667		0,419		0,623	
	9 h	0,941		0,856		0,518		0,449	
0.5 g	3 h	1,375	1,124	0,759	0,669	0,651	0,476	0,430	0,285
	6 h	1,013		0,866		0,559		0,762	
	9 h	1,115		1,030		0,617		0,522	

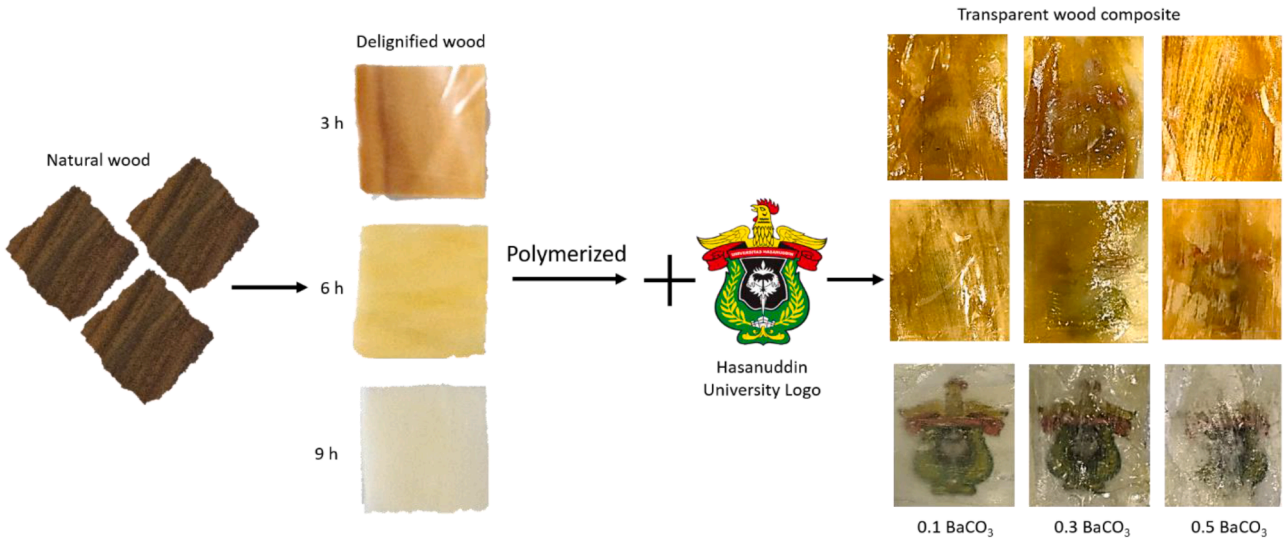

Fig. 3. The transparent shielding film of composite PVA/Gelatin/$BaCO_3$/wood in this study. The Hasanuddin University logo clearly appear behind the shielding indicated high transparency.

Fig. 3 also shows a composite radiation shielding film that has become transparent after polymerization using PVA/Gelatin matrix. The combination between two different types of polymers (PVA/Gelatin) and carbon based (wood) with oxides $BaCO_3$ materials, the new composites could be fabricated with increase the electrochemical sensing performance based on track-etched membranes when polymer was added as reported by Korolkov et al. [46], and significantly improve electronic properties (consequently affects to the transparency performance) compared with that of the individual materials. Transparency testing was done by placing Hasanuddin University logo behind the composite film and photographed. The visual changes can be clearly observed in Fig. 3. The delignification for 9 h shows the most effective transparency compare with other samples. Then, when given the addition of $BaCO_3$, there was a change in film transparency. The more $BaCO_3$ content given, the sheer cloud will form which causes decrease of transparency. Transparent radiation shielding film from

PVA/Gelatin/$BaCO_3$/wood composite shows the best transparency after being delignified for 9 h and with the addition of 0.1 g of $BaCO_3$ content.

Moreover, the addition of metal element also reducing the thickness of composite film from 1.62, 1.43, and 1.23 cm with variations of $BaCO_3$ was 0.1, 0.3, and 0.5 gm, respectively.

3.2. Fourier transform infrared analysis

The FTIR spectra of 4 wood samples (Fig. 4) shows absorption in the wavenumber between 600–3700 cm^{-1}. The characteristic bands at 892 cm^{-1} which is due to C—H bond, 1022 cm^{-1} is ascribed to C—O bond. The appeared band at 1376 cm^{-1} corresponding to C—H bond reformed by cellulose and hemicellulose [64]. The showed band at 1140–1240 cm^{-1} and 930–1117 cm^{-1} are C—O—C bonds [65,66]. At 2802–2997 cm^{-1}, a stretching vibrational band of C—H bond appeared by the methoxyl lignin group and the broad band at 3022–3700 cm^{-1} due to O—H bond [67]. The spectra at 1550–1828 cm^{-1} forms the C═O bond by aromatic and hemicellulose groups and 1245 cm^{-1} forms the C—O bond contributed by lignin [68,69]. The others band at 600–725 and 1510 cm^{-1} form C═C bond contributed by aromatic rings [70,71].

As the heating time increases, absorption peak of C═C bonds and some oxygen in the functional groups were changes due to wood fibers reduced as well as the degradation of chemical compounds such as polysaccharides, hemicellulose, and lignin.

The shifted of C—H and O—H bonds to higher wavenumbers also contributed by the changes of cellulose crystallinity and oxidation of OH groups in hemicellulose [71]. After 9 h delignification, the FTIR spectra shows a shift in absorption peaks to a higher wavenumbers due to the degradation of carbon aromatic groups or lignin content in wood samples or increase oxygen vacancies [70–75].

Polyvinyl alcohol (PVA) have been used as polymer matrices due to the environmentally friendly, easily soluble in water, and good transparency [41,42]. The natural polymer is environmentally friendly such gelatin where easily for production in large scale [43]. The combination of different compounds that have excellent electronic properties leads to create new composite materials which have earned great technological interest in pharmaceutical and industrial fields [44,45]. The addition of gelatin to PVA will produce new composite material which have second phase and affected significantly in improving the electronic properties [76].

3.3. X-ray shielding

Radiation shielding material in the form of PVA/Gelatin/$BaCO_3$/transparent wood composites for the thicknesses of 1.62, 1.43, and 1.25 cm by 0.1, 0.3, and 0.5 gm of $BaCO_3$, respectively. The X-ray shielding ability was tested for the photon energies of 55, 66, 77, and 90 keV by

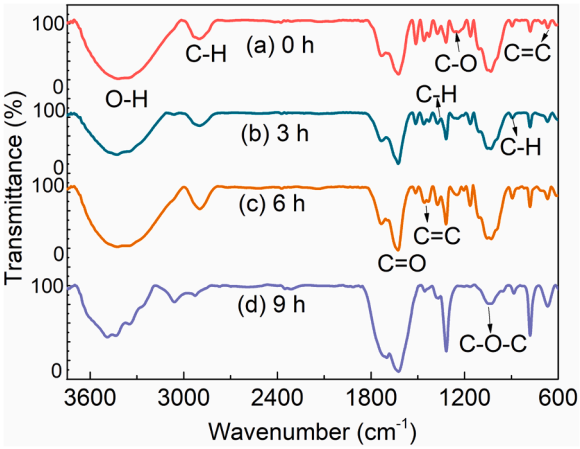

Fig. 4. FTIR spectra of wood with different delignification time.

determine the initial intensity and intensity after radiation or attenuated as shown in Beer-Lambert's equation [77–79]:

$$I = I_o e^{-\mu x} \tag{1}$$

where μ is the linear attenuation coefficient, x is sample thickness, I_o and I are initial intensity and intensity after radiation or radiation attenuated. The linear attenuation coefficient shows interaction probability of photon and radiation shielding sample [79].

Fig. 5 shows the linear attenuation coefficient curve of the PVA/Gelatin/$BaCO_3$/transparent wood shielding. The experimental result with different delignification time given for 3 h (filled square symbol), 6 h (filled circles symbol), and 9 h (filled triangle symbol). The theoretically calculation obtained by XCOM [80] for comparison (circle open symbol). The linear attenuation coefficient decreases as the energy increases from the photon energy. The PVA/Gelatin/$BaCO_3$/transparent wood composite shows the highest linear attenuation coefficient of 1.37463 cm^{-1} at 55 keV with of 0.5 g of $BaCO_3$. This is due to the dominant photoelectric interaction between photons and absorber materials in low energy ranges [8,19,77,81].

Fig. 5 also shows the mass attenuation coefficient curve that can be determined by divided linear attenuation coefficient with the density of PVA/Gelatin/$BaCO_3$/transparent wood composite (ρ) [82]:

$$\mu_m = \frac{\mu}{\rho} \tag{2}$$

From the Fig. 5, Tables 2, and 3 clearly shows that the mass attenuation coefficient decreases along with the increase in photon energy caused by the photoelectric effect [77,83]. When photons are fully absorbed by the absorber material, the major attenuation occurs in this region [84]. After addition of 0.3 and 0.5 g of $BaCO_3$ in PVA/Gelatin/$BaCO_3$/transparent wood composite, the curve shows a sudden change when the photon energy up to 77 keV. This probably due to agglomeration of Ba element in composite [85,86] and the ejected photon from photoelectric effect or photoelectron interact with other atoms around it and Compton interactions might happen at this energy levels [14,49,81,85–88]. This might be led to the instability of experimental and theoretical data (XCOM) at some energy levels. This changes also related to the wood transparency decrease as shown in Fig. 3, in which delignification increase the light attenuation but the metal element makes the transparency become blurred [34,54].

The agglomeration of particle clearly can be seen in SEM image in the Fig. 6, is due to the small size of particles joint together to form big particle indicated that, there is no specific surface morphology. The high delignification time of wood in the synthesized process affected in reducing the surface energy through agglomeration. For Fig. 6**(a)** delignified wood shows composed of many stacked nanorod-like, rod shape, and spherical shape. The addition of $BaCO_3$ oxide for Fig. 6 (b–d) shows the polymer $BaCO_3$ oxide fill the pores and interacted with the cellulose nanofibrils in wood cells. Polymers PVA/Gelatin also penetrate in wood cells which play be more tightly bonded**. It is** clearly agglomeration occurred, and the shape and particle size distribution is ununiform which probably leading to increasing oxygen vacancies as reported recently by Zhang and Li [89] also Yakovenko et al. [61] and Yakovenko et al. [62]. The changes of oxygen content affected in changing the charge state from the initial cations and consequence changes such electrical parameters as dc- and ac-resistivity and band gap [75,90]. The oxygen vacancies also contributed for destroy the grain size and increase unit cell parameter as reported by Kozlovskiy and Zdorovets [91], changes in structure and orientation of the grains lead to the porosity, consequently low mechanical properties. After irradiation, in this case the delignification process, there was point defect and dislocation near the boundaries. The defect due to the oxygen vacancy and will be reinforced by polymer-$BaCO_3$ oxide to maintain the mechanical properties. Trukhanov et al. [92] and Kozlovskiy et al. [93] were mentioned that by the additional various content of metal oxide will influenced to

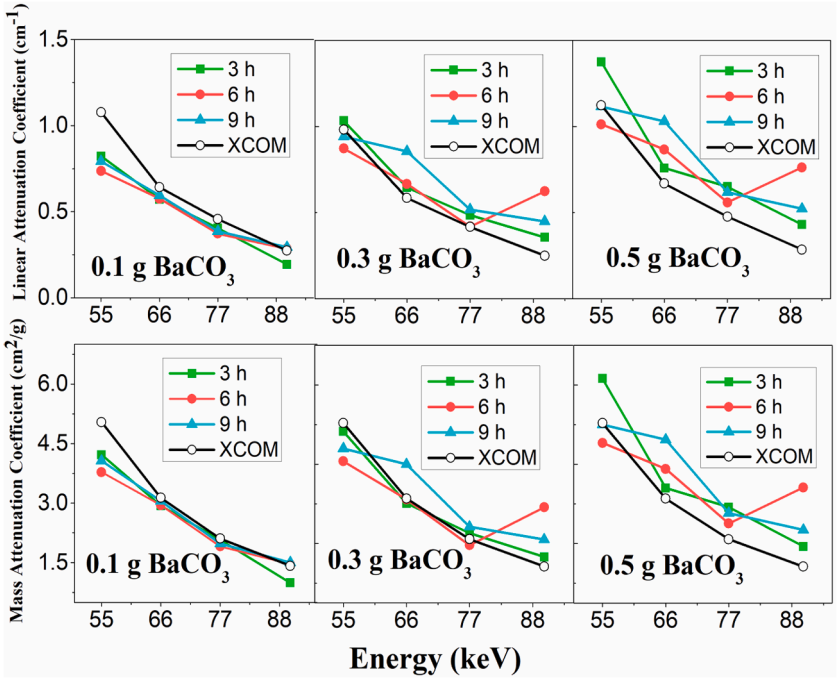

Fig. 5. The experimental value of linear attenuation coefficient (μ) and mass attenuation coefficient (μ_m) for different delignification time and $BaCO_3$ content (filled symbol indicated by 3, 6, and 9 h). We have included theoretical calculation (XCOM database) from NIST (open symbol) for comparison.

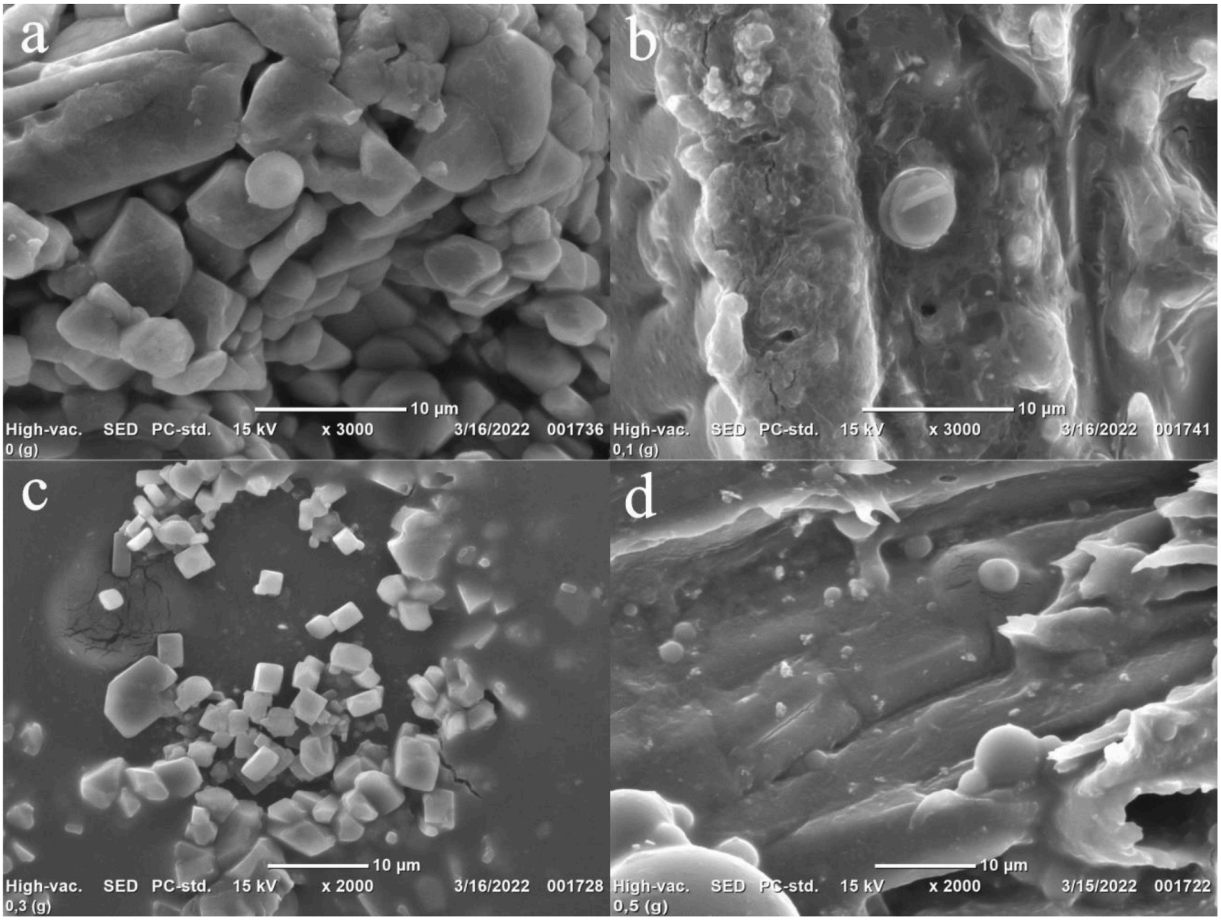

Fig. 6. Scanning electron microscopy (SEM) images of PVA/Gelatin/$BaCO_3$/transparent wood composites with 9 h delignification time of wood, for (a) without $BaCO_3$ and (b) with 0.1 g of $BaCO_3$, (c) 0.3 g of $BaCO_3$, and (d) 0.5 g of $BaCO_3$.

the morphology or physical properties of the composite as well as electronic properties. These phenomenon due to oxygen bonds redistribution as the effect of oxygen vacancies, consequently affected to the magneto and mass transport properties [28,29,72,73,75,94,95].

Fig. 5 also shows increasing of mass attenuation coefficient along with the increase of $BaCO_3$ concentration. This caused by higher interaction between X-ray photon with $BaCO_3$ atoms of the shielding composites due to the denser particles when the addition was increased.

The mass attenuation coefficient causing the decrease of HVL and the varies of the attenuation coefficient also caused by Z (atomic number), composition and thickness of absorber material, and photon energy (E) that been used [49,96].

The radiation shielding ability of PVA/Gelatin/$BaCO_3$/transparent wood composite showed by its half value layer and mean free path value. The Half Value Layer (HVL) is the thickness of a radiation shield that interacts to absorb energy from a radiation source about 50% of its initial intensity [8,79]. An increasing of mass attenuation coefficient leads to a decrease of HVL [88]. HVL can be determined from linear attenuation coefficient (μ) [97], as shown in relation (3):

$$HVL = \frac{\ln 2}{\mu} = \frac{0.693}{\mu} \tag{3}$$

Low HVL proved that the material will absorbed the radiation from photon energy [77,98]. HVL generally approach one at low energy and increasing when the photon energy increase [85,98]. Fig. 7 shows that the trend of HVL increases linearly with increased photon energy and decreases as $BaCO_3$ concentration increases.

In samples with a concentration of 0.5 g $BaCO_3$ in photon energy 55 keV showed the lowest HVL compared to other samples. This proves that the shielding able to absorb most of photon energy as reported Yakovenko et al. [61], and Yakovenko et al. [62], increasing of barium content as well as increasing reflection properties. Therefore, PVA/Gelatin/$BaCO_3$/transparent wood composites can be used as a good radiation shielding material.

Mean Free Path (MFP) is the average distance between two photon interactions in an absorber material or the distance between the intensity attenuated [8,77,99,100]. Mean free path can be determined by relation (4) [77]:

$$MFP = \frac{1}{\mu} \tag{4}$$

Fig. 7 shows that the lowest mean free path of the PVA/Gelatin/$BaCO_3$/transparent wood composite is 0.72747 cm with a concentration of 0.5 g of $BaCO_3$ at photon energy of 55 keV. Low MFP show that photons and samples well-interacting.

Both HVL and MFP shows the different trend when $BaCO_3$ concentration was 0.3 and 0.5 g in the photon energy up to 88 keV. This changes due to the increasing the light attenuation after eliminate lignin content of the wood [34,54], and also affected by K-absorption edge of Ba element and Compton interaction, as explained before [81,85,86]. This phenomenon proves that PVA/Gelatin/$BaCO_3$/transparent wood composite effectively work at low photon energy.

The interaction between photons with atoms and electrons is shown by the atomic cross section and electronic cross section curves Fig. 8). Experimental result with different delignification time given for 3 h (filled square symbol), 6 h (filled circles symbol), and 9 h (filled triangle symbol). The theoretically calculation obtained by XCOM [80] for comparison (circle open symbol). The atomic cross section can be determined by the relation ((5) [82,100,101,102]:

$$(\sigma_{t,a}) = \frac{1}{N_A}\sum_i f_i A_i (\mu_m)_i \tag{5}$$

where N_A, f_i, A_i, $(\mu_m)_i$, are Avogadro's number, fractional abundance, atomic weight of the PVA/Gelatin/$BaCO_3$/transparent wood composite, and mass attenuation coefficient, respectively. Similarly, the relation for electronic cross section is given by:

$$(\sigma_{t,el}) = \frac{1}{N_A}\sum_i \frac{f_i A_i}{Z_i} (\mu_m)_i \tag{6}$$

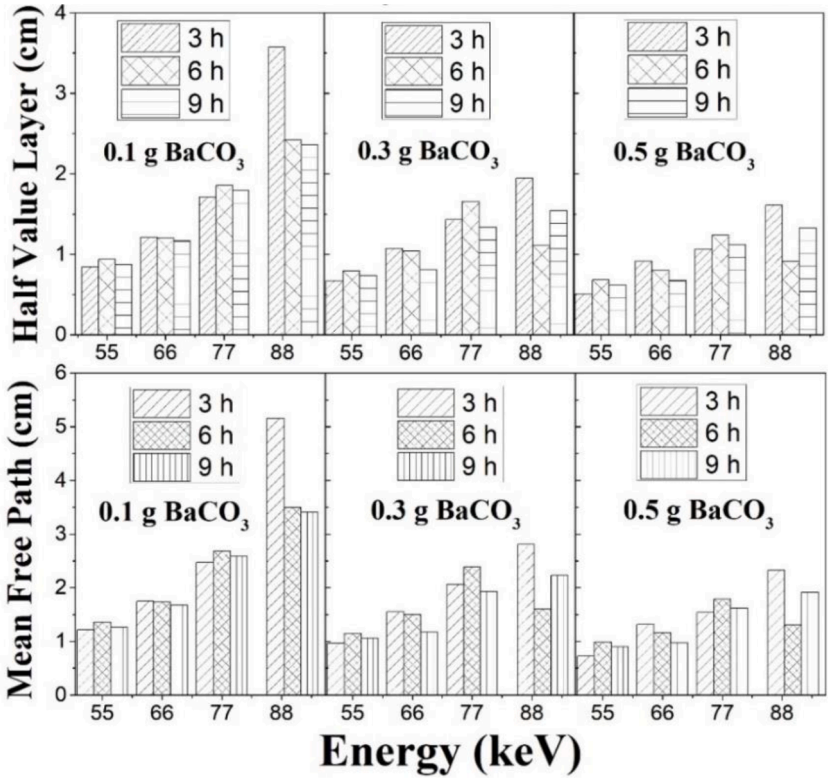

Fig. 7. Half value layer and mean free path for different delignification time and $BaCO_3$ content.

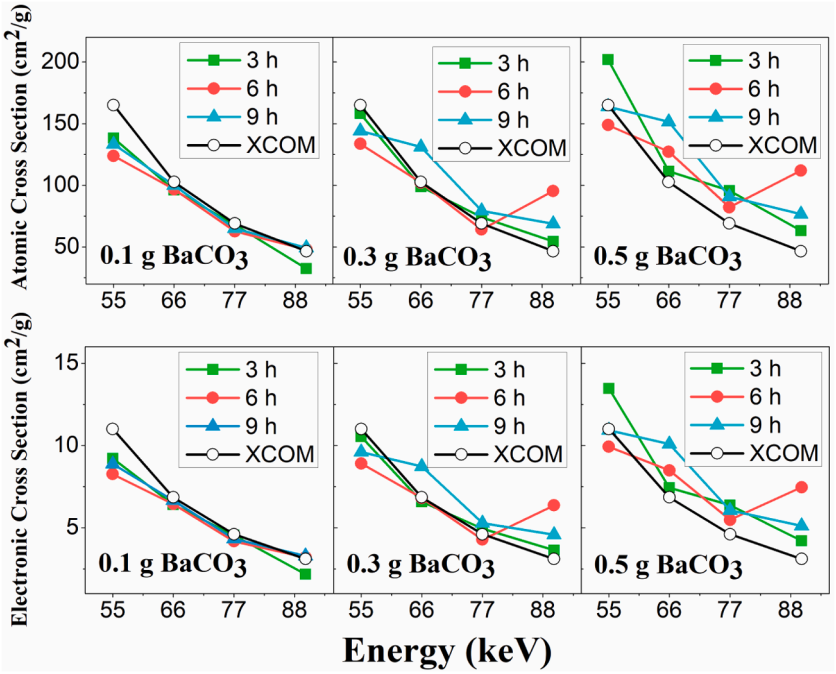

Fig. 8. The experimental value of atomic cross section and electronic cross section for different delignification time and $BaCO_3$ content (filled symbol indicated by 3, 6, and 9 h). We have included theoretical calculation (XCOM database) from NIST (open symbol) for comparison.

where Z_i is the atomic number of contributing element.

As shown in relation (5) and (6), the interaction depends on the atomic number (Z) and electron density (ρ) of the material that has been determined in the mass attenuation coefficient (μ_m). [8,49].

The atomic cross section and electronic cross section shows same trend with linear attenuation coefficient and mass attenuation coefficient curve at photon energy 55 to 90 keV (Fig. 5). When $BaCO_3$ concentration was 0.3 g with energy up to 70 keV, the Compton scattering slightly appear due to high light attenuation [34,54] and makes the theoretical and experimental result has a bit differences [81,85,86].

The interaction between the incoming radiation with delignified wood as shown in Fig. 8. The first rows show the different between natural wood, delignified wood, delignified with additional $BaCO_3$ in two- and three-dimensional view. The second rows show the interaction mechanism by three-dimensional view when the X-ray incoming to the composite and the absorption, reflection, and may few transmissions process have occurred, resulting the electric field in three direction and emission may in visible light or X-ray characteristics. Third rows show two dimensional when considering the atom with the positive ion (Ba^{2+}) is in the middle of free electron. The incoming photon (X-ray) will generate heat from the external field and will produce uniform heating by collision of electric field for uniform atomic structure and for agglomeration will different phenomena.

The transparent wood needs to be reinforced with polymers to obtain good flexibility and mechanical properties due to the lignin content decreases [36,63]. The tensile strength of flexible and transparent shielding shows very low about 0.19 MPa for 0.1 g $BaCO_3$, 0.20 MPa for 0.3 and 0.5 g $BaCO_3$. The mechanical properties of the composite come from the polymer (PVA/Gelatin) [63], where fill the pores and interacted with the cellulose nanofibrils in wood cells. The polymer will increase flexibility and transparency which will be able to bend without breaking the fiber. Polymers also penetrate in wood cells which play be more tightly bonded.

XCOM is theoretical calculation by using software freely online provided by NIST and the result of XCOM data for PVA/Gelatin/$BaCO_3$/transparent wood composite in this study for full energy range as shown in Fig. 10. Photoelectric absorption, coherent and incoherent scattering, total attenuation, and pair production was calculated. In energy ranges below 10 MeV, the photoelectric effect is the major interaction [77] and the trend does not follow the black line but the dashed yellow line; only in certain areas of the curve [81]. When the X-ray beam reaches the radiation shielding, the attenuation will be depends on the chemical composition of the shielding sample and energy of the photon that causes a decrease in radiation intensity. The decreasing of intensity obtained from a combination of scattering and photon absorption [103].

Fig. 10 shows that all interactions decreased when the energy of the photon increased in line with the decrease of mass attenuation coefficient in the sample. The mass attenuation coefficient is a parameter of X-ray penetration when interacting with radiation shielding. The possibility of X-ray interaction per unit length of radiation shield characterizes its linear attenuation coefficient [9]. Compton scattering shows little effect when photons interact with shielding, at an energy of about 60 keV. The compton scattering related linearly with the atomic number of the radiation shielding material [83]. If high energy is used, then Compton scattering may intersect with the interaction of pair production [81].

The photoelectric effect will increase as the concentration of $BaCO_3$ increases, the trend is the same as the mass attenuation coefficient [88]. The effectiveness of radiation shielding will be shown by its mass attenuation coefficient and the thickness of its half value layer [77,98].

4. Conclusions

The delignified wood veneers has been fabricated by treated with hydrogen peroxide for 3, 6, and 9 h to remove the lignin content and showed changing in color of the wood veneer from dark brownish (natural wood) to yellowish (3 h), and then brighter (6 h) to white (9 h). Then, X-ray radiation shielding material in the form of PVA/Gelatin/BaCO3/transparent wood composites also successfully fabricated for the first time with the thicknesses of 1.62, 1.43, and 1.25 cm by 0.1, 0.3, and 0.5 gm of $BaCO_3$, respectively. The X-ray shielding test shows the highest linear attenuation coefficient of 1.37463 cm^{-1} at 55 keV with of 0.5 g of $BaCO_3$. The mass attenuation coefficient increasing linearly along with the increase of $BaCO_3$ concentration. In samples with a concentration of 0.5 g $BaCO_3$ also showed the lowest HVL compared to

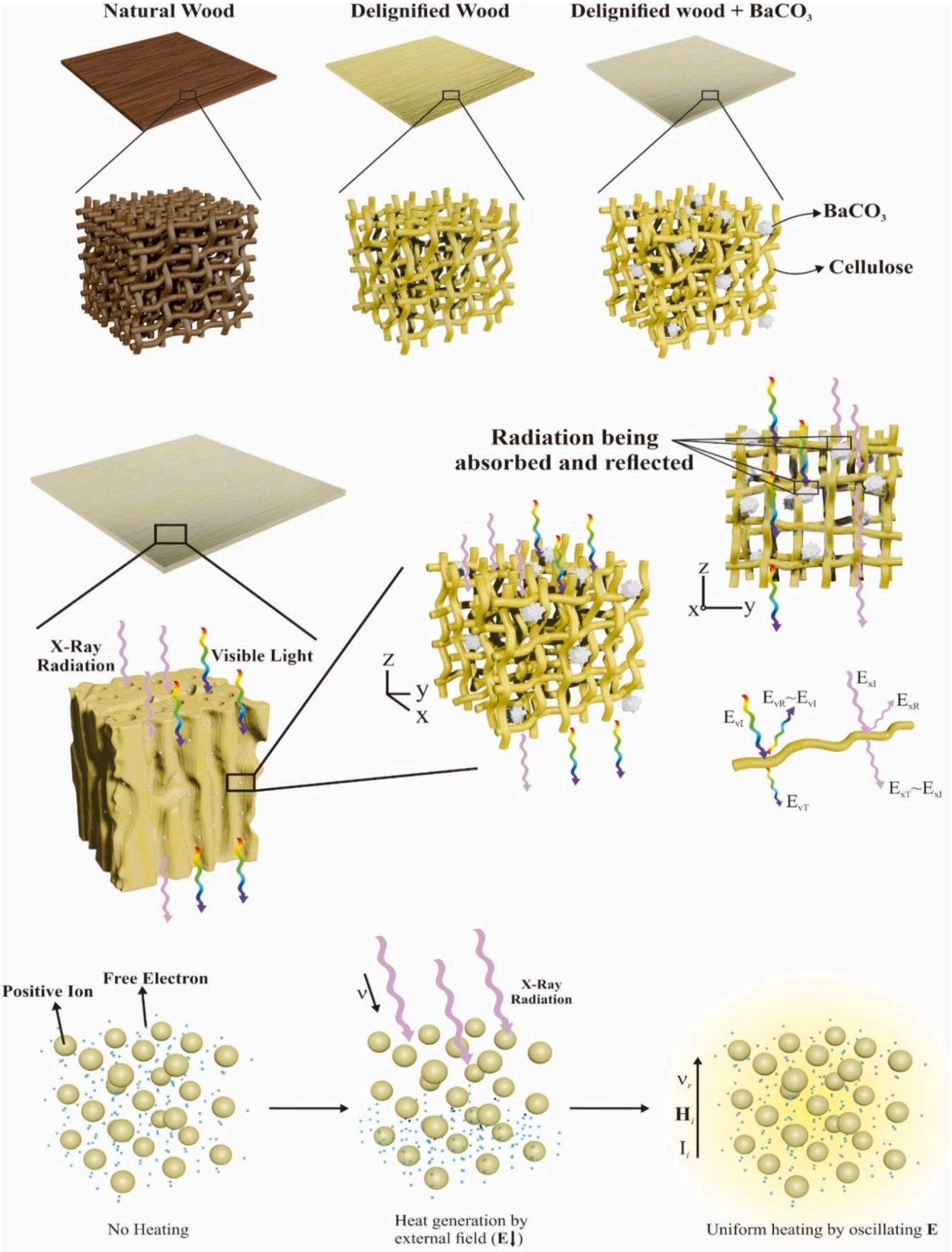

Fig. 9. The schematic illustration for three-dimensional view (first row) of natural wood, delignified wood, and delignified + $BaCO_3$. The second row the interaction mechanism by three-dimensional view when the X-ray incoming and absorption process occurred and resulting the electric field in three directions. Third rows show two dimensional when considering the atoms of the composite is positive ion in the middle of free electron, the incoming photon (X-ray) will generate heat from the external field and will produce uniform heating by collision of electric field for uniform atomic structure.

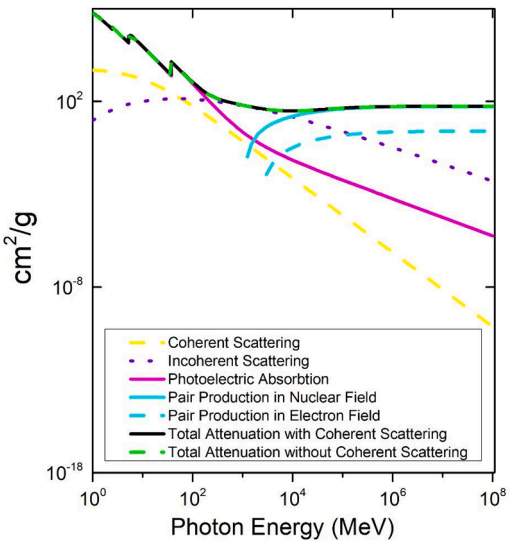

Fig. 10. Derived from XCOM for PVA/Gelatin/$BaCO_3$/transparent wood composite in this study to show full energy range from 10^0 MeV up to 10^8 MeV.

others with 0.72747 cm of mean free path. This proves that the shielding able to absorb most of photon energy and the photons and samples well-interacting. Therefore, PVA/Gelatin/$BaCO_3$/transparent wood composites can be a new opportunity as effective transparent and flexible X-ray radiation shielding application.

Declaration of Competing Interest

The authors declare that they have no known competing financial interests or personal relationships that could have appeared to influence the work reported in this paper.

References

[1] A.N. D'Souza, et al., Role of Bi_2O_3 in altering the structural, optical, mechanical, radiation shielding and thermoluminescence properties of heavy metal oxide borosilicate glasses, J. Non. Cryst. Solids 542 (2020), 120136, https://doi.org/10.1016/j.jnoncrysol.2020.120136. March.

[2] S.C. Kim, K.R. Dong, W.K. Chung, Medical radiation shielding effect by composition of barium compounds, Ann. Nucl. Energy 47 (2012) 1–5, https://doi.org/10.1016/j.anucene.2012.04.014.

[3] C.J. Panetta, et al., Reduced radiation exposure in the cardiac catheterization laboratory with a novel vertical radiation shield, Catheter. Cardiovasc. Interv. 95 (1) (2020) 7–12, https://doi.org/10.1002/ccd.28629.

[4] S. Akbulut Özen, M. Özen, M. Şahin, M. Mertens, Study of the hydrothermal crystallization process of barium titanate by means of X-ray mass attenuation coefficient measurements at an energy of 59.54 keV, Mater. Charact. 129 (2017) 329–335, https://doi.org/10.1016/j.matchar.2017.05.006. May.

[5] K. Günther, et al., Cellulose/inorganic-composite fibers for producing textile fabrics of high X-ray absorption properties, Mater. Chem. Phys. 167 (2015) 125–135, https://doi.org/10.1016/j.matchemphys.2015.10.019.

[6] E. Kalkornsurapranee, et al., Wearable and flexible radiation shielding natural rubber composites: effect of different radiation shielding fillers, Radiat. Phys. Chem. 179 (2021), 109261, https://doi.org/10.1016/j.radphyschem.2020.109261. November 2020.

[7] X. Jiang, X. Zhu, C. Chang, S. Liu, X. Luo, X-ray shielding structural and properties design for the porous transparent $BaSO_4$/cellulose nanocomposite membranes, Int. J. Biol. Macromol. 139 (2019) 793–800, https://doi.org/10.1016/j.ijbiomac.2019.07.186.

[8] N. Nagaraja, H.C. Manjunatha, L. Seenappa, K.N. Sridhar, H.B. Ramalingam, Radiation shielding properties of silicon polymers, Radiat. Phys. Chem. 171 (2020), 108723, https://doi.org/10.1016/j.radphyschem.2020.108723. January.

[9] S. Aggrey-Smith, K. Preko, F.W. Owusu, J.K. Amoako, Study of radiation shielding properties of selected tropical wood species for X-rays in the 50-150 keV Range, Open Access J. Sci. Technol. 4 (2016) 1–8, https://doi.org/10.11131/2016/101150.

[10] S.A. Hashemi, S.M. Mousavi, R. Faghihi, M. Arjmand, S. Sina, A.M. Amani, Lead oxide-decorated graphene oxide/epoxy composite towards X-ray radiation shielding, Radiat. Phys. Chem. 146 (2018) 77–85, https://doi.org/10.1016/j.radphyschem.2018.01.008. July 2017.

[11] M.I. Sayyed, et al., Extensive study of newly developed highly dense transparent $PbO-WO_3-BaO-Na_2O-B_2O_3$ glasses for radiation shielding applications, J. Non Cryst. Solids 521 (2019), 119521, https://doi.org/10.1016/j.jnoncrysol.2019.119521. JuneOct.

[12] N.J. AbuAlRoos, N.A. Baharul Amin, R. Zainon, Conventional and new lead-free radiation shielding materials for radiation protection in nuclear medicine: a review, Radiat. Phys. Chem. 165 (2019), https://doi.org/10.1016/j.radphyschem.2019.108439. July.

[13] J.G. Pounds, R.W. Leggett, The ICRP age-specific biokinetic model for lead: validations, empirical comparisons, and explorations, Environ. Health Perspect. 106 (6) (1998) 1505–1511, https://doi.org/10.1289/ehp.98106s61505. SUPPL.

[14] M.H. Hazlan, M. Jamil, R.M. Ramli, N.Z. Noor Azman, X-ray attenuation characterisation of electrospun Bi_2O_3/PVA and WO_3/PVA nanofibre mats as potential X-ray shielding materials, Appl. Phys. A 124 (7) (2018) 497, https://doi.org/10.1007/s00339-018-1915-8. Jul.

[15] A. Güngör, K. Akbay, D. Yaşar, T. Özdemir, Flexible X/Gamma ray shielding composite material of EPDM rubber with bismuth trioxide: mechanical, thermal investigations and attenuation tests, Prog. Nucl. Energy 106 (2018) 262–269, https://doi.org/10.1016/j.pnucene.2018.03.021. March.

[16] S.N. Yılmaz, İ.K. Akbay, T. Özdemir, A metal-ceramic-rubber composite for hybrid gamma and neutron radiation shielding, Radiat. Phys. Chem. 180 (2021), https://doi.org/10.1016/j.radphyschem.2020.109316.

[17] A.G. Nuñez-Briones, et al., Preparation of PVC/Bi_2O_3 composites and their evaluation as low energy X-ray radiation shielding, Radiat. Phys. Chem. 179 (2020) (2021), 109198, https://doi.org/10.1016/j.radphyschem.2020.109198. April.

[18] D.I. Tishkevich, et al., Correlation of the synthesis conditions and microstructure for Bi-based electron shields production, J. Alloy. Compd. 749 (2018) 1036–1042, https://doi.org/10.1016/j.jallcom.2018.03.288.

[19] M. Jamil, M.H. Hazlan, R.M. Ramli, N.Z. Noor Azman, Study of electrospun PVA-based concentrations nanofibre filled with Bi_2O_3 or WO_3 as potential X-ray shielding material, Radiat. Phys. Chem. 156 (2019) 272–282, https://doi.org/10.1016/j.radphyschem.2018.11.018. Mar.

[20] D.I. Tishkevich, et al., Function composites materials for shielding applications: correlation between phase separation and attenuation properties, J. Alloy. Compd. 771 (2019) 238–245, https://doi.org/10.1016/j.jallcom.2018.08.209.

[21] V. Thongpool, A. Phunpueok, N. Barnthip, S. Jaiyen, $BaSO_4$/polyvinyl alcohol composites for radiation shielding, Appl. Mech. Mater. 804 (2015) 3–6, https://doi.org/10.4028/www.scientific.net/amm.804.3. May 2017.

[22] S. Jaiyen, A. Phunpueok, V. Thongpool, Determination of radiation attenuation coefficients of $BaSO_4$/PVC and $BaSO_4$/PS for X-ray shielding, J. Phys. Conf. Ser. 1380 (1) (2019), 012133, https://doi.org/10.1088/1742-6596/1380/1/012133. Nov.

[23] L. Gholamzadeh, H. Sharghi, M.K. Aminian, Synthesis of barium-doped PVC/Bi_2WO_6 composites for X-ray radiation shielding, Nucl. Eng. Technol. 54 (1) (2022) 318–325, https://doi.org/10.1016/j.net.2021.07.045.

[24] A.V. Trukhanov, et al., Evolution of structure and magnetic properties for $BaFe_{11.9}Al_{0.1}O_{19}$ hexaferrite in a wide temperature range, J. Magn. Magn. Mater. 426 (2017) 487–496, https://doi.org/10.1016/j.jmmm.2016.10.140.

[25] M.V. Zdorovets, A.L. Kozlovskiy, D.I. Shlimas, D.B. Borgekov, Phase transformations in FeCo – Fe_2CoO_4/Co_3O_4-spinel nanostructures as a result of thermal annealing and their practical application, J. Mater. Sci. Mater. Electron. (2021), https://doi.org/10.1007/s10854-021-06226-5.

[26] M.A. Almessiere, et al., Strong correlation between Dy^{3+} concentration, structure, magnetic and microwave properties of the $[Ni_{0.5}Co_{0.5}](DyxFe_{2-x})O_4$ nanosized ferrites, J. Ind. Eng. Chem. 90 (2020) 251–259, https://doi.org/10.1016/j.jiec.2020.07.020.

[27] A. Thakur, et al., Synthesis of barium ferrite nanoparticles using rhizome extract of Acorus Calamus: characterization and its efficacy against different plant phytopathogenic fungi, Nano Struct. Nano Objects 24 (2020), 100599, https://doi.org/10.1016/j.nanoso.2020.100599.

[28] T. Zubar, et al., Features of the growth processes and magnetic domain structure of NiFe nano-objects, J. Phys. Chem. C 123 (44) (2019) 26957–26964, https://doi.org/10.1021/acs.jpcc.9b06997.

[29] T.I. Zubar, et al., Control of growth mechanism of electrodeposited nanocrystalline NiFe films, J. Electrochem. Soc. 166 (6) (2019) D173–D180, https://doi.org/10.1149/2.1001904jes.

[30] P. Gairola, S.P. Gairola, V. Kumar, K. Singh, S.K. Dhawan, Barium ferrite and graphite integrated with polyaniline as effective shield against electromagnetic interference, Synth. Met. 221 (2016) 326–331, https://doi.org/10.1016/j.synthmet.2016.09.023.

[31] A. Yakubu, Z. Abbas, A. Sirajo, Attenuation and shielding performance of wood-polymer composites synthesized via melt-blend technique, OALib 07 (02) (2020) 1–11, https://doi.org/10.4236/oalib.1105444.

[32] W. Poltabtim, E. Wimolmala, T. Markpin, N. Sombatsompop, V. Rosarpitak, K. Saenboonruang, X-ray shielding, mechanical, physical, and water absorption properties of wood/PVC composites containing bismuth oxide, Polymers 13 (13) (2021) 2212, https://doi.org/10.3390/polym13132212 (Basel)Jul.

[33] O.E. Özkan, Investigation of the radiation shielding properties of black pine wood impregnated with boric acid, Kastamonu Üniv. Orman Fak. Derg. 20 (2) (2020) 200–207, https://doi.org/10.17475/kastorman.801770.

[34] N.A. Muhammad, Isnaeni, D. Tahir, Optical properties of wood by laser spectroscopy, J. Phys. Conf. Ser. 1341 (8) (2019), 082019, https://doi.org/10.1088/1742-6596/1341/8/082019. Oct.

[35] Y. Li, E. Vasileva, I. Sychugov, S. Popov, L. Berglund, Optically transparent wood: recent progress, opportunities, and challenges, Adv. Opt. Mater. 6 (14) (11, 2018), 1800059, https://doi.org/10.1002/adom.201800059. Jul.

[36] Y. Wu, J. Wu, F. Yang, C. Tang, Q. Huang, Effect of H2O2 bleaching treatment on the properties of finished transparent wood, Polymers 11 (5) (2019) 1–13, https://doi.org/10.3390/polym11050776 (Basel).

[37] A.N. Subba Rao, G.B. Nagarajappa, S. Nair, A.M. Chathoth, K.K. Pandey, Flexible transparent wood prepared from poplar veneer and polyvinyl alcohol, Compos. Sci. Technol. 182 (2019), 107719, https://doi.org/10.1016/j.compscitech.2019.107719. JuneSep.

[38] Y. Li, X. Gu, H. Gao, J. Li, Photoresponsive wood composite for photoluminescence and ultraviolet absorption, Constr. Build. Mater. 261 (119984) (2020) 1–7, https://doi.org/10.1016/j.conbuildmat.2020.119984.

[39] E. Jungstedt, C. Montanari, S. Östlund, L. Berglund, Mechanical properties of transparent high strength biocomposites from delignified wood veneer, Compos. Part A Appl. Sci. Manuf. 133 (2020), 105853, https://doi.org/10.1016/j.compositesa.2020.105853. November 2019.

[40] J. Wu, Y. Wu, F. Yang, C. Tang, Q. Huang, J. Zhang, Impact of deligni fi cation on morphological, optical and mechanical properties of transparent wood, Compos. Part A 117 (2019) 324–331, https://doi.org/10.1016/j.compositesa.2018.12.004. June 2018.

[41] W. Wu, H. Tian, A. Xiang, Influence of polyol plasticizers on the properties of polyvinyl alcohol films fabricated by melt processing, J. Polym. Environ. 20 (1) (2012) 63–69, https://doi.org/10.1007/s10924-011-0364-7.

[42] H. Chandrappa, R.F. Bhajantri, , Ranjitha, Shwetha, N. Prarthana, Simple fabrication of PVA-ATE (Amaranthus tricolor leaves extract) polymer biocomposites: an efficient UV-Shielding material for organisms in terrestrial and aquatic ecosystems, Opt. Mater. 109 (2020), 110204, https://doi.org/10.1016/j.optmat.2020.110204 (Amst).July.

[43] N. Karmaker, et al., Fabrication and characterization of PVA-gelatin-nano crystalline cellulose based biodegradable film: effect of gamma radiation, J. Res. Updat. Polym. Sci. 8 (2019) 7–14, https://doi.org/10.6000/1929-5995.2019.08.02.

[44] M. Navarro-Lozoya, M.S. Kennedy, D. Dean, J.I. Rodriguez-Devora, Development of phantom material that resembles compression properties of human brain tissue for training models, Materialia 8 (Dec. 2019), 100438, https://doi.org/10.1016/j.mtla.2019.100438. August.

[45] M.A. Anugrah, et al., Composite gelatin/Rhizophora SPP particleboards/PVA for soft tissue phantom applications, Radiat. Phys. Chem. 173 (2020), 108878, https://doi.org/10.1016/j.radphyschem.2020.108878. March.

[46] I.V. Korolkov, N. Zhumanazar, Y.G. Gorin, A.B. Yeszhanov, M.V. Zdorovets, Enhancement of electrochemical detection of Pb^{2+} by sensor based on track-etched membranes modified with interpolyelectrolyte complexes, J. Mater. Sci. Mater. Electron. 31 (22) (2020) 20368–20377, https://doi.org/10.1007/s10854-020-04556-4.

[47] M.A. Anugrah, S. Suryani, I. Mutmainna, A.N. Fahri, D. Tahir, Structural and bonding characteristic of composite gelatine-PVA-Zn for phantom breast cancer applications, in: Proceedings of the AIP Conference Proceedings 2219, 2020, 080002, https://doi.org/10.1063/5.0003008. May.

[48] B.M. Abunahel, R.M. Ramli, K.M. Quffa, N.Z.N. Azman, Effect of nanofibrous porosity on the X-ray attenuation properties of electrospun n-Bi_2O_3/epoxy–polyvinyl alcohol (PVA) nanofiber mats, Appl. Phys. A 124 (8) (2018) 540, https://doi.org/10.1007/s00339-018-1975-9. Aug.

[49] B.M. Abunahel, I.S. Mustafa, N.Z. Noor Azman, Characteristics of X-ray attenuation in nano-sized bismuth oxide/epoxy-polyvinyl alcohol (PVA) matrix composites, Appl. Phys. A 124 (12) (2018) 828, https://doi.org/10.1007/s00339-018-2254-5. Dec.

[50] A.A. Ebnalwaled, A.M. Ismaiel, Developing novel UV shielding films based on PVA/Gelatin/0.01CuO nanocomposite: on the properties optimization using γ-irradiation, Meas. J. Int. Meas. Confed. 134 (2019) 89–100, https://doi.org/10.1016/j.measurement.2018.10.062. Feb.

[51] M. Zhu, et al., Highly anisotropic, highly transparent wood composites, Adv. Mater. 28 (26) (2016) 5181–5187, https://doi.org/10.1002/adma.201600427.

[52] X. Wang, et al., Large-size transparent wood for energy-saving building applications, ChemSusChem 11 (23) (2018) 4086–4093, https://doi.org/10.1002/cssc.201801826.

[53] J. Qin, et al., Optimization of delignification process for efficient preparation of transparent wood with high strength and high transmittance, Vacuum 158 (26) (2018) 158–165, https://doi.org/10.1016/j.vacuum.2018.09.058.

[54] Y. Li, Q. Fu, S. Yu, M. Yan, L. Berglund, Optically transparent wood from a nanoporous cellulosic template: combining functional and structural performance, Biomacromolecules 17 (4) (2016) 1358–1364, https://doi.org/10.1021/acs.biomac.6b00145.

[55] Q. Xia, et al., Solar-assisted fabrication of large-scale, patternable transparent wood, Sci. Adv. 7 (5) (2021) 1–8, https://doi.org/10.1126/sciadv.abd7342.

[56] H. Li, X. Guo, Y. He, R. Zheng, A green steam-modified delignification method to prepare low-lignin delignified wood for thick, large highly transparent wood composites, J. Mater. Res. 34 (6) (2019) 932–940, https://doi.org/10.1557/jmr.2018.466.

[57] C. Montanari, Y. Li, H. Chen, M. Yan, L.A. Berglund, Transparent wood for thermal energy storage and reversible optical transmittance, ACS Appl. Mater. Interfaces 11 (22) (2019) 20465–20472, https://doi.org/10.1021/acsami.9b05525.

[58] H.S. Yaddanapudi, N. Hickerson, S. Saini, A. Tiwari, Fabrication and characterization of transparent wood for next generation smart building applications, Vacuum 146 (2017) 649–654, https://doi.org/10.1016/j.vacuum.2017.01.016. January.

[59] Z. Yu, et al., Transparent wood containing CsXWO3 nanoparticles for heat-shielding window applications, J. Mater. Chem. A 5 (13) (2017) 6019–6024, https://doi.org/10.1039/c7ta00261k.

[60] Y. Wu, et al., Study on the colorimetry properties of transparent wood prepared from six wood species, ACS Omega 5 (4) (2020) 1782–1788, https://doi.org/10.1021/acsomega.9b02498.

[61] O.S. Yakovenko, et al., Effect of magnetic fillers and their orientation on the electrodynamic properties of BaFe12-xGaxO19 (x = 0.1–1.2)—epoxy composites with carbon nanotubes within GHz range, Appl. Nanosci. 10 (12) (2020) 4747–4752, https://doi.org/10.1007/s13204-020-01477-w.

[62] O.S. Yakovenko, et al., Electromagnetic properties of carbon nanotube/bafe12−xgaxo19/epoxy composites with random and oriented filler distributions, Nanomaterials 11 (11) (2021) 1–12, https://doi.org/10.3390/nano11112873.

[63] M. Frey, L. Schneider, K. Masania, T. Keplinger, I. Burgert, Delignified wood-polymer interpenetrating composites exceeding the rule of mixtures, ACS Appl. Mater. Interfaces 11 (38) (2019) 35305–35311, https://doi.org/10.1021/acsami.9b11105.

[64] A.L. Missio, B.D. Mattos, P.H.G. Cademartori, T.V. Lourençon, J. Labidi, D. A. Gatto, The effect of oleoresin tapping on physical and chemical properties of Pinus elliottii wood, Sci. For. Sci. 43 (107) (2015) 721–732.

[65] W.D. Ding, A. Koubaaa, A. Chaala, Dimensional stability of methyl methacrylate hardened hybrid poplar wood, BioResources 7 (1) (2012) 504–520, https://doi.org/10.15376/biores.7.1.0504-0520.

[66] C. Liang, H. Qiu, P. Song, X. Shi, J. Kong, J. Gu, Ultra-light MXene aerogel/wood-derived porous carbon composites with wall-like 'mortar/brick' structures for electromagnetic interference shielding, Sci. Bull. 65 (8) (2020) 616–622, https://doi.org/10.1016/j.scib.2020.02.009.

[67] X. Yin, A. Huang, S. Zhang, R. Liu, F. Ma, Identification of three dalbergia species based on differences in extractive components, Molecules 23 (9) (2018) 2163, https://doi.org/10.3390/molecules23092163. Aug.

[68] J. Li, et al., Direct and complete utilization of agricultural straw to fabricate all-biomass films with high-strength, high-haze and UV-shielding properties, Carbohydr. Polym. 223 (2019), 115057, https://doi.org/10.1016/j.carbpol.2019.115057. July.

[69] J. de O. Lopes, R.A. Garcia, N.D. de Souza, Infrared spectroscopy of the surface of thermally-modified teak juvenile wood, Maderas Cienc. Tecnol. 20 (4) (2018) 737–746, https://doi.org/10.4067/S0718-221X2018005041901.

[70] Z. Wang, X. Han, X. Han, Z. Chen, S. Wang, J. Pu, MXene/wood-derived hierarchical cellulose scaffold composite with superior electromagnetic shielding, Carbohydr. Polym. 254 (2021), 117033, https://doi.org/10.1016/j.carbpol.2020.117033. August.

[71] A.F. Dias Júnior, R.N. de Oliveira, X. Deglise, N.D. de Souza, J.O. Brito, Infrared spectroscopy analysis on charcoal generated by the pyrolysis of Corymbia. Citriodora wood, Matéria 24 (3) (2019), https://doi.org/10.1590/s1517-707620190003.0700 (Rio Janeiro).

[72] P. Dey, T.K. Nath, Effect of grain size modulation on the magneto- and electronic-transport properties of La0.7 Ca0.3 Mn O3 nanoparticles: The role of spin-polarized tunneling at the enhanced grain surface, Phys. Rev. B Condens. Matter Mater. Phys. 73 (21) (2006) 1–14, https://doi.org/10.1103/PhysRevB.73.214425.

[73] V.V. Rylkov, et al., Magnetic Metal-Nonstoichiometric Oxide Nanocomposites: Structure, Transport, and Memristive Properties, Elsevier Inc., 2018.

[74] M.D. McCluskey, Defects in ZnO, defects in advanced electronic materials and novel low dimensional structures, in: Electronic and Optical Materials, Woodhead Publishing Series, 2018, pp. 1–25.

[75] X.D. Zhou, H.U. Anderson, Defect chemistry of ternary oxides, Mater. Energy Convers. Devices A Vol. Woodhead Publ. Ser. Electron. Opt. Mater. (2005) 235–259, https://doi.org/10.1533/9781845690915.2.235.

[76] Z. Yang, H. Peng, W. Wang, T. Liu, Crystallization behavior of poly(ε-caprolactone)/layered double hydroxide nanocomposites, J. Appl. Polym. Sci. 116 (5) (2010) 2658–2667, https://doi.org/10.1002/app.

[77] S.A. Issa, H.M.H. Zakaly, M. Pyshkina, M.Y.A. Mostafa, M. Rashad, T.S. Soliman, Structure, optical, and radiation shielding properties of PVA–BaTiO3 nanocomposite films: an experimental investigation, Radiat. Phys. Chem. 180 (Mar. 2021), 109281, https://doi.org/10.1016/j.radphyschem.2020.109281.

[78] M.V. Muthamma, S.G. Bubbly, S.B. Gudennavar, K.C.S. Narendranath, Poly(vinyl alcohol)–bismuth oxide composites for X-ray and γ-ray shielding applications, J. Appl. Polym. Sci. 136 (37) (2019) 1–10, https://doi.org/10.1002/app.47949.

[79] A.A. Elbary, M. Tammam, Physical and mechanical properties of polyamide 6/polystyrene (PA6/PS) reinforced by PbO 2 composites for X-ray shielding, J. Thermoplast. Compos. Mater. (Sep. 2019) 1–19, https://doi.org/10.1177/0892705719872524.

[80] L. Gerward, N. Guilbert, K.B. Jensen, H. Levring, WinXCom - a program for calculating X-ray attenuation coefficients, Radiat. Phys. Chem. 71 (3–4) (2004) 653–654, https://doi.org/10.1016/j.radphyschem.2004.04.040.

[81] C.G. Hernandez-Murillo, J.R. Molina Contreras, L.A. Escalera-Velasco, H.A. de Leon-Martínez, J.A. Rodriguez-Rodriguez, H.R. Vega-Carrillo, X-ray and gamma ray shielding behavior of concrete blocks, Nucl. Eng. Technol. 52 (8) (2020) 1792–1797, https://doi.org/10.1016/j.net.2020.01.007.

[82] P.S. Kore, P.P. Pawar, Measurements of mass attenuation coefficient, effective atomic number and electron density of some amino acids, Radiat. Phys. Chem. 98 (2014) 86–91, https://doi.org/10.1016/j.radphyschem.2013.12.038.

[83] L. Seenappa, H.C. Manjunatha, B.M. Chandrika, K.N. Sridhar, C. Hanumantharayappa, Gamma, X-ray and neutron interaction parameters of Mg–Gd–Y–Zn–Zr alloys, Radiat. Phys. Chem. 150 (2018) 199–206, https://doi.org/10.1016/j.radphyschem.2018.06.026. June.
[84] K.A. Mahmoud, F.I. El-Agawany, O.L. Tashlykov, E.M. Ahmed, Y.S. Rammah, The influence of BaO on the mechanical and gamma /fast neutron shielding properties of lead phosphate glasses, Nucl. Eng. Technol (2021), https://doi.org/10.1016/j.net.2021.06.005 xxxx.
[85] M.S. Al-Buriahi, et al., Structure, optical, gamma-ray and neutron shielding properties of NiO doped B_2O_3–BaCO3–Li2O3 glass systems, Ceram. Int. 46 (2) (2020) 1711–1721, https://doi.org/10.1016/j.ceramint.2019.09.144.
[86] B.O. El-bashir, M.I. Sayyed, M.H.M. Zaid, K.A. Matori, Comprehensive study on physical, elastic and shielding properties of ternary BaO-Bi_2O_3-P_2O_5 glasses as a potent radiation shielding material, J. Non. Cryst. Solids 468 (2017) 92–99, https://doi.org/10.1016/j.jnoncrysol.2017.04.031. May.
[87] W. Hongtong, et al., Development of gadolinium doped calcium phosphate oxyfluoride glasses for X-ray shielding materials, Mater. Today Proc. 5 (6) (2018) 14063–14068, https://doi.org/10.1016/j.matpr.2018.02.062.
[88] N. Chanthima, et al., Development of BaO–ZnO–B_2O_3 glasses as a radiation shielding material, Radiat. Phys. Chem. 137 (2017) 72–77, https://doi.org/10.1016/j.radphyschem.2016.03.015.
[89] J. Zhang, J. Li, The oxygen vacancy defect of ZnO/NiO nanomaterials improves photocatalytic performance and ammonia sensing performance, Nanomaterials 12 (3) (2022), https://doi.org/10.3390/nano12030433.
[90] A. Fujimoto, et al., Negative magnetoresistance of indium tin oxide nanoparticle thin films grown by chemical thermolysis, J. Phys. Soc. Jpn. 82 (2) (2013) 1–7, https://doi.org/10.7566/JPSJ.82.024710.
[91] A.L. Kozlovskiy, M.V. Zdorovets, Study of hydrogenation processes in radiation-resistant nitride ceramics, J. Mater. Sci. Mater. Electron. 31 (14) (2020) 11227–11237, https://doi.org/10.1007/s10854-020-03671-6.
[92] S.V. Trukhanov, et al., Magnetic properties of $La_{0.70}Sr_{0.30}MnO_{2.85}$ anion-deficient manganite under hydrostatic pressure, JETP Lett. 83 (1) (2006) 33–36, https://doi.org/10.1134/S0021364006010085.
[93] A. Kozlovskiy, K. Egizbek, M.V Zdorovets, M. Ibragimova, Evaluation of the efficiency of detection and capture of manganese in aqueous solutions of FeCeO x nanocomposites doped with Nb2O5, Sensors 20 (2020) 1–15, https://doi.org/10.3390/s20174851.
[94] M.A. Almessiere, et al., Tuning the structure, magnetic, and high frequency properties of Sc-doped $Sr_{0.5}Ba_{0.5}Sc_xFe_{12-xO19}/NiFe_2O_4$ hard/soft nanocomposites, Adv. Electron. Mater. 8 (2) (2022), https://doi.org/10.1002/aelm.202101124.
[95] S.V. Trukhanov, et al., Magnetotransport properties and mechanism of the A-site ordering in the Nd-Ba optimal-doped manganites, J. Low Temp. Phys. 149 (2007) 185–199, https://doi.org/10.1007/s10909-007-9507-6.
[96] S. Jayakumar, T. Saravanan, J. Philip, Preparation, characterization and x-ray attenuation property of gd2 o3-based nanocomposites, Appl. Nanosci. 7 (8) (2017) 919–931, https://doi.org/10.1007/s13204-017-0631-6.
[97] M. Elsafi, M.I. Sayyed, A.H. Almuqrin, M.M. Gouda, A.M. El-khatib, Analysis of particle size on mass dependent attenuation capability of bulk and nanoparticle PbO radiation shields, Results Phys 26 (2021), 104458, https://doi.org/10.1016/j.rinp.2021.104458.
[98] Nurhasmi, et al., Geopolimer concrete for radiation shielding application, Mater. Sci. Forum 966 (2019) 41–47, https://doi.org/10.4028/www.scientific.net/MSF.966.41. AugustAug.
[99] Y.S. Rammah, M.S. Al-Buriahi, A.S. Abouhaswa, B_2O_3–$BaCO_3$–Li_2O_3 glass system doped with Co_3O_4: Structure, optical, and radiation shielding properties, Phys. B Condens. Matter 576 (2020), 411717, https://doi.org/10.1016/j.physb.2019.411717.
[100] R. Bagheri, A. Khorrami Moghaddam, H. Yousefnia, Gamma ray shielding study of barium–bismuth–borosilicate glasses as transparent shielding materials using MCNP-4C Code, XCOM program, and available experimental data, Nucl. Eng. Technol. 49 (1) (2017) 216–223, https://doi.org/10.1016/j.net.2016.08.013.
[101] M.A. Anugrah, S. Ilyas, D. Tahir, Gelatin/poly (vinyl alcohol)/inorganic filler composites for phantom breasts, Mater. Chem. Phys. 262 (2021), https://doi.org/10.1016/j.matchemphys.2021.124333. September 2020.
[102] H. Baltaş, Ş. Çelik, U. Çevik, E. Yanmaz, Measurement of mass attenuation coefficients and effective atomic numbers for MgB2 superconductor using X-ray energies, Radiat. Meas. 42 (1) (2007) 55–60, https://doi.org/10.1016/j.radmeas.2006.08.005.
[103] O. Gurler, U. Akar Tarim, Determination of radiation shielding properties of some polymer and plastic materials against gamma-rays, Acta Phys. Pol. A 130 (1) (2016) 236–238, https://doi.org/10.12693/APhysPolA.130.236.